Structural, electrical, and optical properties of ZnInO alloy thin films*

Cai Xi-Kun(才玺坤), Yuan Zi-Jian(原子健), Zhu Xia-Ming(朱夏明), Wang Xiong(王 雄), Zhang Bing-Po(张兵坡), Qiu Dong-Jiang(邱东江), and Wu Hui-Zhen(吴惠桢)†

Department of Physics, State Key Laboratory of Silicon Materials, Zhejiang University, Hangzhou 310027, *China*

(Received 9 February 2011; revised manuscript received 4 May 2011)

Indium zinc oxide (IZO) thin films with different percentages of In content (In/[In+Zn]) are synthesized on glass substrates by magnetron sputtering, and the structural, electrical and optical properties of IZO thin films deposited at different In_2O_3 target powers are investigated. IZO thin films grown at different In_2O_3 target sputtering powers show evident morphological variation and different grain sizes. As the In_2O_3 sputtering power rises, the grain size becomes larger and electrical mobility increases. The film grown with an In_2O_3 target power of 100 W displays the highest electrical mobility of 13.5 $cm\cdot V^{-1}\cdot s^{-1}$ and the lowest resistivity of 2.4×10^{-3} $\Omega\cdot$cm. The average optical transmittance of the IZO thin film in the visible region reaches 80% and the band gap broadens with the increase of In_2O_3 target power, which is attributed to the increase in carrier concentration and is in accordance with Burstein–Moss shift theory.

Keywords: indium-zinc oxide, magnetron sputtering, In content, optical properties, electrical properties

PACS: 61.66.Dk, 68.55.ag, 73.61.Ga, 78.66.Hf **DOI:** 10.1088/1674-1056/20/10/106103

1. Introduction

Transparent conducting oxides (TCOs) have attracted significant attention due to their high transparency in the visible region and high electrical conductivity. TCOs are widely used in many fields such as flat panel displays, optoelectronic devices and solar cells. Most studies of TCO films concentrate on Sn-doped In_2O_3 (ITO) films because of their good electrical and optical properties. Recently, there has been a growing interest in the development of new transparent conducting oxides such as indium zinc oxide (IZO),[1,2] zinc tin oxide (ZTO),[3] and aluminium zinc oxide (AZO).[4] Compared with ITO film, IZO film has been shown to be a promising material due to its higher conductivity, higher optical transparency and smoother surface.[1] Therefore, IZO films may provide an alternative to traditional ITO films used in optoelectronic applications. IZO thin films have been deposited by various processes including metal-organic chemical-vapour deposition (MOCVD),[2] pulsed-laser deposition,[5] magnetron sputtering,[6] and sol–gel processing.[7] Among these processes, magnetron sputtering has the advantages of a relatively low-cost process and a low deposition temperature.

It is known that intrinsic binary ZnO material shows low electron concentration and poor electrical conductivity, which restricts its use in electronic devices. In this paper, by introducing In into ZnO films we produce IZO thin film with a high electron concentration and high electrical conductivity. The IZO films were deposited by radio frequency (RF) magnetron sputtering through co-sputtering of two targets with ZnO and In_2O_3. Compared with the growth technique using a single IZO target,[8] it is more flexible to adjust and control the properties of IZO films and we can conveniently obtain IZO films with different compositions by changing one or both of the two target powers. We investigate the dependence of physical properties of IZO thin films on In_2O_3 target power.

2. Experiment

IZO thin films were deposited by RF magnetron sputtering through co-sputtering of ZnO and In_2O_3 targets on glass substrates. High purity (99.999%) argon was used as sputtering gas during the deposition process. The chamber base pressure was ap-

*Project supported by the National Natural Science Foundation of China (Grant No. 10974174) and the Natural Science Foundation of Zhejiang Province of China (Grant Nos. Z6100117, Z1110057, and Y4080171).

†Corresponding author. E-mail: hzwu@zju.edu.cn

© 2011 Chinese Physical Society and IOP Publishing Ltd

proximately 6.5×10^{-5} Pa and the targets were pre-sputtered for 20 min before deposition. A flow rate of Ar gas was 6 sccm and working pressure was 1.0 Pa. All the films were grown at room temperature. Glass substrates were cleaned in an ultrasonic bath with acetone, alcohol and deionized water separately, and then dried with high purity nitrogen gas blowing. We deposite IZO thin films at a fixed ZnO target power of 100 W and In_2O_3 target powers of 100 W, 60 W, 40 W, and 20 W, separately.

The crystal structural properties of the IZO thin films were analysed by a D/max-rA X-ray diffractometer (XRD) using Cu Kα radiation (λ = 1.5406 Å, 1 Å=0.1 nm). The surface morphology and EDX measurement were characterized by a Hitachi S4800 field-emission scanning electron microscope (FESEM). The film thicknesses were measured by an XP-1 Stylus Profilometer. The resistivity, the electrical mobility and the carrier concentration of the films were obtained by Hall effect measurement using the van der Pauw configuration with an HL5500 apparatus in which indium electrodes were used for Ohmic contacts. The optical transmittance was measured by a UV-3150 spectrophotometer.

3. Results and discussion

3.1. Structural properties

Figure 1 shows the scanning electron microscope (SEM) images of the IZO thin films at different In_2O_3 target powers. The SEM images reflect the transition of the surface morphology from 9.5% to 37.9% of In content. In Fig. 1(a), the film grown at an In_2O_3 target power of 20 W is composed of granular grains with size varying from 20 nm to 60 nm. For the film grown at an In_2O_3 target power of 40 W, the film is comprised of compactly arranged grains with high grain density and small sizes compared with the film grown at 20 W. When the In_2O_3 target power is increased to 60 W, it is shown that some small grains gather together, forming larger grain groups as shown in Fig. 1(c). As can be seen in Fig. 1(d), the grains are distributed desultorily and void spaces occur among the grains, which could be regarded as the enhancement of the gathering phenomenon.

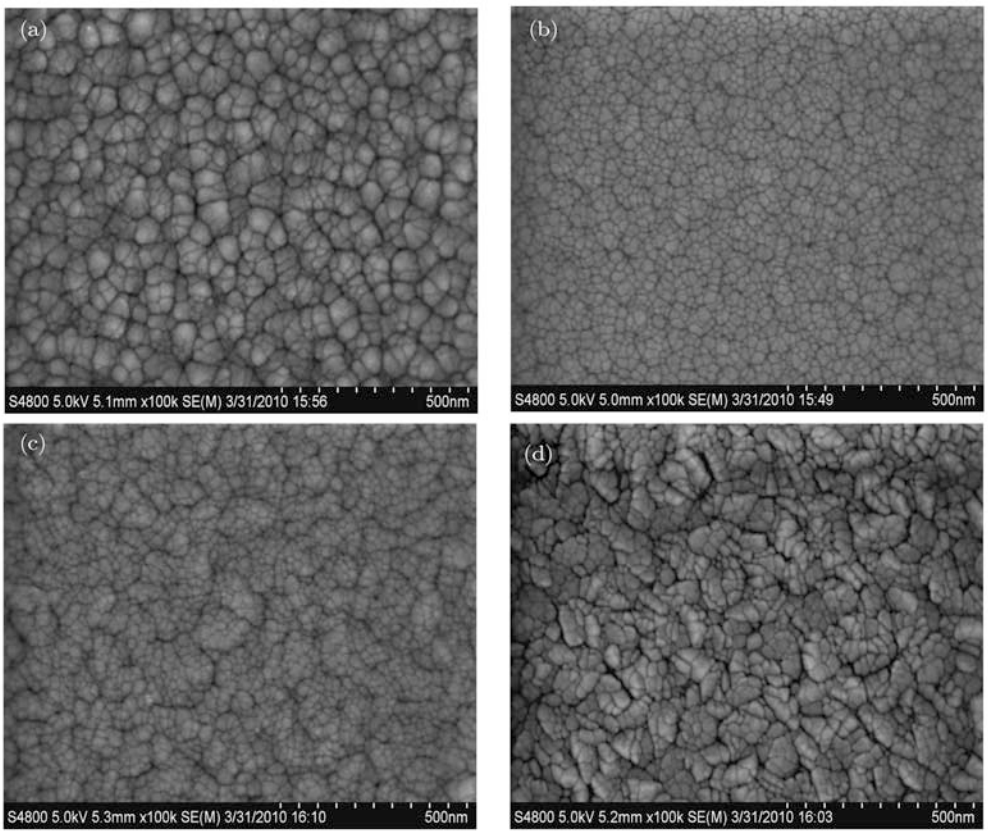


Fig. 1. SEM images of the IZO thin films deposited at different sputtering powers on the In_2O_3 target: (a) 20 W, (b) 40 W, (c) 60 W, and (d) 100 W.

Figure 2 shows the XRD patterns of pure ZnO, pure In_2O_3, and IZO alloy thin films deposited at different In_2O_3 target powers, i.e. 100 W, 60 W, 40 W, and 20 W, separately. The broad peaks around 23° are attributed to the diffraction of glass substrates. The crystal planes of pure ZnO and pure In_2O_3 are labeled and the peaks of IZO alloy thin films are marked as 1#, 2#, 3#, and 4#. From Fig. 2 we can see that all the films are polycrystalline. Peak 1# is located between 31° and 34°, just within the diffraction angles of In_2O_3 (222) and ZnO (002) peak positions. It is obvious that the IZO film grown with In_2O_3 target power of 20 W has three small peaks, which correspond to (100), (002) and (101) peaks of ZnO with the incorporation of a small amount of In_2O_3. Compared with the peak of pure ZnO film, the (002) peak becomes weak. From the composition analysis below, we see that the In content of the film is 0.095. Therefore, at low In content, the film has a ZnO-type structure. When the In_2O_3 target power rises, the ZnO (100) and (101) peaks become weak and eventually disappear, while peaks 3# and 4# tend to become stronger. We can assume that the hexagonal ZnO phase has evolved into a cubic In_2O_3 phase as the increase of In content of the film. Peaks 3# and 4# can be regarded as (422) and (026) peaks of cubic In_2O_3 by qualitative analysis. However, the XRD pattern of pure In_2O_3 does not show these two peaks. So the IZO alloy films may have a more complex structure like a layered $Zn_kIn_2O_{k+3}$ type structure[9,10] and the details of structure of IZO film may need other more complicated structural characterizations that are beyond the scope of this paper. As the increase of In content, larger In atoms replace the smaller Zn atoms in the crystal, leading the observed peaks (1#∼4#) to shift towards low 2θ angles. In addition, it is proved by the calculated layer spacing distance d through using Bragg's equation as listed in Table 1, and the composition analysis is shown in Fig. 3. The grain size given in Table 1 is calculated by the Scherrer's formula $D = 0.9\lambda/\beta\cos\theta$ and the grain size of the IZO thin film increases from 8.6 nm to 15.1 nm with the rise of In_2O_3 target power. It is interesting to note that the grain size seen from SEM is different from the grain size determined by XRD analysis. This suggests the grains observed in SEM are probably polycrystalline domains formed by clusters of nanocrystallites.[11]

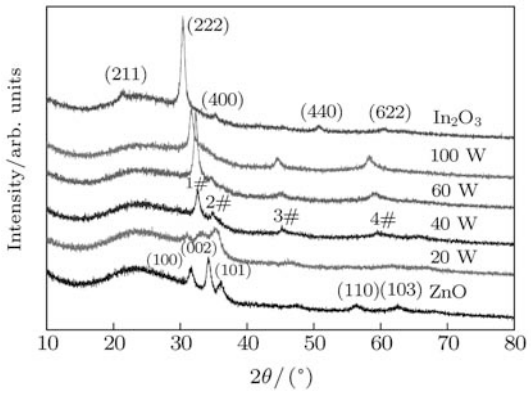


Fig. 2. XRD patterns of IZO thin films deposited at different In_2O_3 target powers.

Table 1. XRD data of peak 1#.

In_2O_3 target power/W	2θ/(°)	FWHM/(°)	d/A	Grain size/nm
20	33.20	0.967	2.6966	8.6
40	32.62	0.635	2.7432	13.0
60	32.32	0.57	2.7680	14.5
100	31.62	0.546	2.8277	15.1

Figure 3 shows the variations of In content (In/[In+Zn]) of IZO thin films and the deposition rate with In_2O_3 target power. The In/(In+Zn) composition ratios are measured by EDX. As shown in Fig. 3, both the deposition rate and the In content almost linearly increase with the rise of In_2O_3 target power. The deposition rate changes from 1.2 A/s to 2 A/s, while the In content varies from 9.5% to 37.9% as sputtering power for In_2O_3 target increases from 20 W to 100 W.

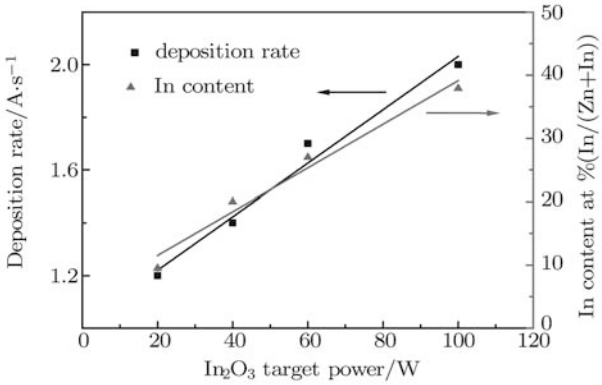


Fig. 3. Deposition rate and In content (In/[In+Zn]) versus In_2O_3 target power, respectively.

3.2. Electrical properties

Table 2 and figure 4 show the dependences of electrical resistivity, electrical mobility and carrier concentration on In_2O_3 target power. The resistivity decreases from 7.7×10^{-2} Ω·cm to 2.4×10^{-3} Ω·cm with the increase of In_2O_3 target power, while the carrier concentration increases from 4.8×10^{19} cm^{-3} to 2×10^{20} cm^{-3}. The film grown with In_2O_3 target power of 100 W displays the highest electrical mobility of 13.5 $cm\cdot V^{-1}\cdot s^{-1}$ and the lowest resistivity of 2.4×10^{-3} Ω·cm. From the results of the composition analysis above, the films are Zn-rich. This may suggest that the presence of indium in the zinc oxide lattice effectively acts as a donor by supplying a single free electron,[12] leading the carrier concentration to increase with the rise of In_2O_3 target power. The electrical mobility changes from 1.7 $cm^2\cdot V^{-1}\cdot s^{-1}$ to 13.5 $cm^2\cdot V^{-1}\cdot s^{-1}$ with the increase of In_2O_3 target power. In order to determine the scattering mechanism, we calculate the mean free path for electrons in IZO films. The mean free path for electrons in n-type metallic oxide is[12−14]

$$l_e = h/2q(3n/\pi)^{1/3}\mu, \tag{1}$$

where n is the carrier concentration, μ is the electrical mobility, and q is the fundamental unit of electric charge. We obtain a range from 0.13 nm to 1.61 nm, much smaller than the grain size from 8.6 nm to 15.1 nm. So the influence of grain boundary scattering on electrical mobility can be ignored. As sputtering power on the In_2O_3 target increases, more In atoms are incorporated into the alloys, thereby influencing the functionality of the thin films. In^{3+} with a longer orbit radius is hard to capture the conductive electron due to the lower binding force, which may subdue the scattering of free electrons by the ions and so the motion of free electrons in the alloy is less influenced than that of Zn^{2+}. Hence the macroscopically observed electrical mobility is enhanced as In composition increases.

Table 2. Electrical properties of IZO thin films.

In_2O_3 target power/W	Resistivity /Ω·cm	Mobility /$cm^2\cdot V^{-1}\cdot s^{-1}$	Carrier concentration/cm^{-3}
20	0.077	1.7	4.8×10^{19}
40	0.060	1.6	6.4×10^{19}
60	0.016	4.3	9×10^{19}
100	0.0024	13.5	2×10^{20}

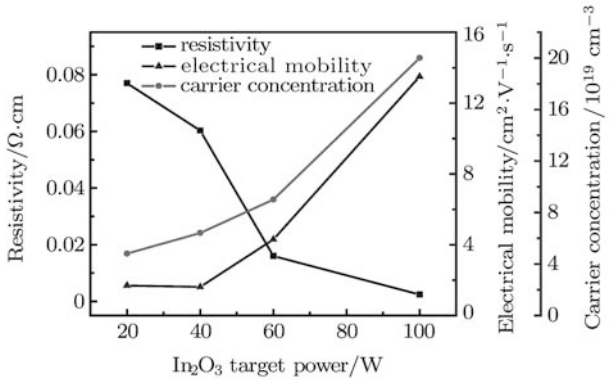


Fig. 4. Dependences of resistivity, electrical mobility, and carrier concentration on In_2O_3 target power.

3.3. Optical properties

Figure 5 shows the optical transmission spectra in the visible region for the IZO thin films deposited at different In_2O_3 target powers. The oscillations from 450 nm to 800 nm are due to the film interference. The average transmittance of the film reaches 80%. The inset displays the curves of $(\alpha h\nu)^2$ versus photon energy. It follows two equations[15]

$$\alpha = \ln\left(\frac{1}{T}\right)/d, \tag{2}$$

$$(\alpha h\nu)^2 = A(h\nu - E_g), \tag{3}$$

where α is the absorption coefficient, T is the transmittance, d is the film thickness, A is a constant for the direct transition and E_g is the optical band gap. By fitting the transmission spectra, the optical band gaps of the IZO thin films deposited at different In_2O_3 target powers are 3.18 eV, 3.20 eV, 3.24 eV, and 3.31 eV. It is obvious that the band gap broadens with the increase of In_2O_3 target power, which can be attributed to the well-known Burstein–Moss shift[16,17] due to the increase in carrier concentration with the increase of In_2O_3 target power. The Burstein–Moss shift ΔE_{MB} in the free electron approximation is given as[18]

$$\Delta E_{MB} = \frac{h^2}{8\pi^2 m^*}(3\pi^2 n_e)^{2/3}, \tag{4}$$

where m^* is the electron effective mass and n_e is the electron carrier concentration. We can obtain the calculated value of n_e by using the equation. Assuming that $m^* = 0.3m_e$[18,19] and the intrinsic band gap

is 3.01 eV for IZO,[20] $\Delta E_{\rm MB}$ can be obtained to be 0.17 eV, 0.19 eV, 0.23 eV, and 0.30 eV for IZO films deposited with different In_2O_3 powers. The comparison of the calculated and measured carrier concentration data versus In_2O_3 power is indicated in Fig. 6. The calculated data matches well with the measured one when In_2O_3 power is below 60 W. Larger band gap energies ranging from 3.5 eV to 3.8 eV have also been reported[19,21] and it is caused by a big Burstein–Moss shift due to much higher conductivity.[22]

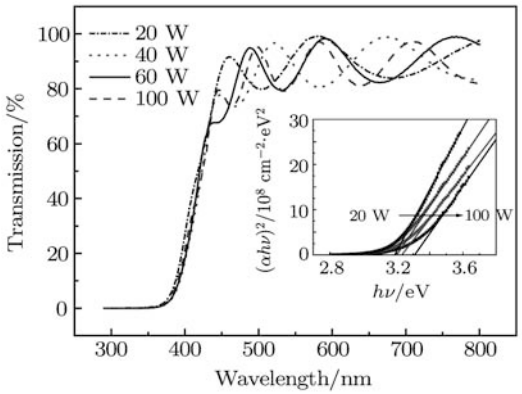


Fig. 5. Optical transmission spectra of IZO thin films deposited at different In_2O_3 target powers. The inset shows the curves of $(\alpha h\nu)^2$ versus photon energy.

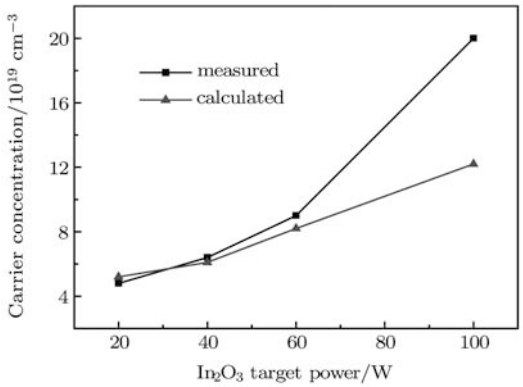


Fig. 6. Calculated and measured carrier concentrations each as a function of In_2O_3 target power.

4. Conclusions

IZO thin films were deposited by RF magnetron sputtering with targets of ZnO and In_2O_3. The films with different quantities of In are polycrystalline and the grain size becomes larger as In_2O_3 sputtering power rises. The resistivity of IZO thin film decreases with the increase of In_2O_3 target power, while the carrier concentration and the electrical mobility increase. The film grown with an In_2O_3 target power of 100 W has the highest electrical mobility of 13.5 cm·V^{-1}·s^{-1} and the lowest resistivity of 2.4×10^{-3} Ω·cm. So the IZO films with higher electrical mobility and lower resistivity can be obtained by increasing the In_2O_3 target power. The average optical transmittance of IZO thin film in the visible region reaches 80%. The band gap broadens with the increase of In_2O_3 target power, which is attributed to the increase in carrier concentration and in accordance with Burstein–Moss shift theory.

References

[1] Sasabayashi T, Ito N, Nishimura E, Kon M, Song P K, Utsumi K, Kaijo A and Shigesato Y 2003 *Thin Solid Films* **445** 219

[2] Wang A C, Dai J Y, Cheng J Z, Chudzik M P, Marks T J, Chang R P H and Kannewurf C R 1998 *Appl. Phys. Lett.* **73** 327

[3] Holmelund E, Schou J, Tougaard S and Larsen N B 2002 *Appl. Surf. Sci.* **197** 467

[4] Zhong W W, Liu F M, Cai L G, Zhou C C, Ding P and Zhang H A 2010 *Chin. Phys.* B **19** 107306

[5] Naghavi N, Rougier A, Marcel C, Guery C, Leriche J B and Tarascon J M 2000 *Thin Solid Films* **360** 233

[6] Lim W, Wang Y L, Ren F, Norton D P, Kravchenko I I, Zavada J M and Pearton S J 2008 *Appl. Surf. Sci.* **254** 2878

[7] Luna-Arredondo E J, Maldonado A, Asomoza R, Acosta D R, Melendez-Lira M A and Olvera M D L 2005 *Thin Solid Films* **490** 132

[8] Aw K C, Tsakadze Z, Lohani A and Mhaisalkar S 2009 *Scr. Mater.* **60** 48

[9] Dupont L, Maugy C, Naghavi N, Guery C and Tarascon J M 2001 *J. Sol. St. Ch.* **158** 119

[10] Naghavi N, Marcel C, Dupont L, Rougier A, Leriche J B and Guery C 2000 *J. Mater. Chem.* **10** 2315

[11] Natarajan G, Daniels S, Cameron D C, O'Reilly L, Mitra A, McNally P J, Lucas O F, Kumar R T R, Reid I and Bradley A L 2006 *J. Appl. Phys.* **100** 033520

[12] Park J B, Park S H and Song P K 2010 *J. Phys. Chem. Sol.* **71** 669

[13] Wohlmuth W and Adesida I 2005 *Thin Solid Films* **479** 223

[14] Tuna O, Selamet Y, Aygun G and Ozyuzer L 2010 *J. Phys.* D **43** 055402

[15] Park S H, Park S E, Lee J C, Song P K and Lee J H 2009 *J. Kor. Phys. Soc.* **54** 1344

[16] Elangovan E, Marques A, Pimentel A, Martins R and Fortunato E 2008 *Vacuum* **82** 1489

[17] Kim H M, Ahn J S and Je K C 2003 *Jpn. J. Appl. Phys.* Part 1 **42** 5714

[18] Dixit A, Sudakar C, Naik R, Naik V M and Lawes G 2009 *Appl. Phys. Lett.* **95** 192105

[19] Ito N, Sato Y, Song P K, Kaijio A, Inoue K and Shigesato Y 2006 *Thin Solid Films* **496** 99

[20] Orikasa Y, Hayashi N and Muranaka S 2008 *J. Appl. Phys.* **103** 113703

[21] Pan H C, Shiao M H, Su C Y and Hsiao C N 2005 *J. Vac. Sci. Technol.* A **23** 1187

[22] Leenheer A J, Perkins J D, van Hest M F A M, Berry J J, O'Hayre R P and Ginley D S 2008 *Phys. Rev.* B **77** 115215